Instrumentation for Ionized Space Environments: New High Time Resolution Instrumental Modes of Mutual Impedance Experiments

Luca Bucciantini, P. Henri, P. Dazzi, G. Wattieaux, F. Lavorenti, Xavier Vallières, J Y Brochot, F. Colin, M C Katrougkalou, G. Vengeons, et al.

JGR Space Physics

METHOD

10.1029/2022JA031055

Key Points:

- New mutual impedance instrumental modes (chirp and multi-spectral) for higher time resolution measurements are defined, tested and validated
- The time resolution of mutual impedance measurements is improved by 20 times and the required onboard computing resources are reduced by 20%
- New fast mutual impedance instrumental procedures are tested and validated using 1D-1V Vlasov-Poisson simulations and plasma chamber tests

Correspondence to:

L. Bucciantini,
luca.bucciantini@cnrs.fr

Citation:

Bucciantini, L., Henri, P., Dazzi, P., Wattieaux, G., Lavorenti, F., Vallières, X., et al. (2023). Instrumentation for ionized space environments: New high time resolution instrumental modes of mutual impedance experiments. *Journal of Geophysical Research: Space Physics*, *128*, e2022JA031055. https://doi.org/10.1029/2022JA031055

Received 28 SEP 2022
Accepted 19 JAN 2023

Instrumentation for Ionized Space Environments: New High Time Resolution Instrumental Modes of Mutual Impedance Experiments

L. Bucciantini[1], P. Henri[1,2], P. Dazzi[1,3], G. Wattieaux[4], F. Lavorenti[2,5], X. Vallières[1], J. Y. Brochot[1], F. Colin[1], M. C. Katrougkalou[6,7], G. Vengeons[1], T. Lecas[1], and O. Le Duff[1]

[1]Laboratoire de Physique et Chimie de l'Environnement et de l'Espace (LPC2E), CNRS, Université d'Orléans, Orléans, France, [2]Laboratoire Lagrange, OCA, UCA, CNRS, Nice, France, [3]Laboratoire d'Études Spatiales et d'Instrumentation en Astrophysique (LESIA), Paris Observatory, Paris, France, [4]Laboratoire Plasma et Conversion d'Energie (LAPLACE), CNRS, Université de Toulouse, Toulouse, France, [5]Dipartimento di Fisica, Università di Pisa, Pisa, Italy, [6]Institute de Recherche en Astrophysique et Planétologie (IRAP), Toulouse, France, [7]Royal Institute of Technology (KTH), Stockholm, Sweden

Abstract Mutual impedance experiments are in situ plasma diagnostic techniques for the identification of the plasma density and the electron temperature. Different versions of mutual impedance instruments were included in past and present space missions (e.g., Rosetta, BepiColombo, JUICE and Comet Interceptor). New versions are currently being devised to fit the strong mass, volume and power constraints on nanosatellite platforms for future multi-point space missions. In this study, our goal is to define and validate two new instrumental modes (i.e., chirp and multi-spectral modes) to improve the time resolution of the experiment with respect to typical mutual impedance instrumental modes (i.e., frequency sweep). Higher time resolution measurements are expected to simplify the integration of mutual impedance experiments onboard nanosatellite platforms by facilitating antenna sharing between different experiments. The investigation is performed both (a) numerically, using a 1D-1V electrostatic full kinetic Vlasov-Poisson model and, (b) experimentally, with laboratory tests using a vacuum chamber and a plasma source. From a plasma diagnostic point of view, we find that both the chirp and multi-spectral modes provide measurements identical to the (reference) frequency sweep mode. From an instrumental point of view, multi-spectral measurements are faster than frequency sweep measurements but they require larger amounts of onboard computing resources (i.e., larger power consumption). Chirp measurements, instead, outperform frequency sweep measurements both in terms of measurement duration (20 times faster) and onboard processor usage (20% less).

1. Introduction

Mutual impedance (MI) experiments are in situ plasma diagnostic instrumental techniques used to determine the local plasma density and electron temperature. Different versions of MI experiments have been selected for past (Bahnsen et al., 1988; Béghin & Debrie, 1972; Béghin et al., 1982; Décréau et al., 1978; Grard, 1997; Pottelette et al., 1975; Pottelette & Storey, 1981; Storey et al., 1969) and present space exploration missions. We here recall the RPC-MIP instrument (Trotignon et al., 2007) onboard the ESA mission Rosetta, the PWI/AM2P experiment (Kasaba et al., 2020; Trotignon et al., 2006) onboard the ESA-JAXA BepiColombo mission, the RPWI/MIME experiment onboard the ESA mission JUICE and the DFP/COMPLIMENT instrument onboard the ESA mission Comet Interceptor (Snodgrass & Jones, 2019). New preliminary versions of MI instruments for future nanosatellite space missions are being developed.

Despite the expertise built over the past decades on the use of large satellite platforms for in situ space exploration, small platforms (e.g., nanosatellites) recently sparked the interest of the scientific community. As an example, the Comet Interceptor mission will investigate a pristine comet entering for the first time the solar system using three satellite platforms: one main (large) satellite supported by two (smaller) nanosatellites.

Why should we choose small satellites over larger ones?

On the one hand, large satellites can accommodate several payload instruments thanks to their significant volumes. Because of their complex architecture and varied set of sub-systems, these platforms are typically very expensive. Therefore, they are used for single-satellite missions (e.g., single-point measurements) which allow for local investigations of the plasma environment while ignoring the status of the global system at different locations.

On the other hand, small satellites typically accommodate a very limited amount of payload instruments due to mass, volume, and power consumption constraints. Because of their few components, such single platforms typically correspond to low costs. For a given capitalized cost, it enables one to use several small platforms, thus facilitating multi-satellite missions to provide multi-point simultaneous observations of physical phenomena acting on different (e.g., electron, ion, fluid) spatial scales (Retinò et al., 2021).

Using several small satellite platforms for future multi-point missions, we expect to complement the understanding of the space environment provided by large platforms, for both space weather monitoring and planetary exploration missions.

However, not all the sub-systems previously designed for large satellites are suitable for small platform applications. This is the case for MI instruments, for which past and present instrumental versions do not match the strong constraints of small satellites. Therefore, new versions of MI instrument are currently being developed to comply with these constraints. For this purpose, effort is put into (a) miniaturizing the instrument's electronics and (b) simplifying the system architecture. This is not sufficient to install the instrument on small platforms because a significant part of the mass and volume of MI instrument is associated with its electric antennas and their support structure. Miniaturization of these components is not possible because it would result in significant modifications of MI measurements. Therefore, we propose to follow a different strategy: since other experiments for in situ plasma diagnostic use similar antennas, we propose to reduce the overall mass and volume of the satellite payload by having the antennas shared between different experiments. Thus, instead of putting effort on the miniaturization of the MI antennas, we are focusing on (c) integrating the MI instrument with other plasma diagnostic instruments. The drawback to sharing the same antennas among different experiments is that the simultaneous use of the same integrated components by different experiments is not always possible. As a consequence, each experiment has limited available time to perform its measurements and shared scheduling between integrated experiments is required. Since this would limit the range of dynamic processes the instrument can observe, we need to improve its time resolution to both ensure the observation of the fast processes perturbing the environment and facilitate the integration with other instruments.

Although small satellites facilitate multi-point missions, they are associated to critical technical challenges, especially for scientific electric instruments.

The deployable booms of small satellites are typically very short, at most of the order of 1 m. This means that electric instruments are deployed near the platform, which is the source of different spurious electric perturbations to the measurements. First, electric devices installed on the satellite generate spurious electric signals that perturb the environment and, therefore, electric measurements performed nearby. Second, inhomogeneous plasma regions (i.e., plasma sheath) envelope the satellite platform as a consequence of spacecraft plasma interaction processes. Instruments deployed near the platform are placed near the satellite's plasma sheath, that is known to perturb in situ plasma diagnostic measurements.

On top of that, small satellites are associated with small charging times. This means that their ground electric potential is very sensitive to the currents collected from the plasma and, therefore, a fixed ground potential cannot always be ensured by the platform during the measurements. This is an issue for electric instruments because a varying ground potential can have significant effects on the measurements (Ranvier et al., 2019).

In the following, we neglect the impact of spurious electric signals on MI measurements, and we focus on the reduced time resolution of MI experiments related to antenna sharing. The study of the repercussion that short deployable booms have on MI measurements is left to future investigations.

In this context, we define and validate two new experimental procedures to improve MI experiment time resolution. These procedures correspond to two new instrumental modes (the so-called chirp mode and multi-spectral mode). The measurements of these two modes are validated against those of a reference mode (the so-called frequency sweep mode) typically used in past (e.g., the Rosetta mission) and current (e.g., BepiColombo) space missions. We note that all future MI instruments, both for small or large satellites applications, will benefit from a higher time resolution that will allow for the observation of faster processes.

The two new MI instrumental modes are investigated both numerically (Section 3.1) by means of 1D-1V Vlasov-Poisson numerical simulations (Henri et al., 2010; Mangeney et al., 2002), and experimentally (Section 3.2) by means of plasma chamber validation tests. Numerical simulations and experimental tests have different goals.

Numerical simulations model a simplified interaction between MI experiments and the surrounding plasma. They are used to obtain the (theoretical) instrumental response of the two new MI modes and to ensure it corresponds to that of typical MI experiments. After the theoretical equivalence between the modes is ensured, plasma chamber tests are used to validate the new modes in a representative ionospheric-like environment.

This document is organized as follows. In Section 2 we describe in detail the MI instrumental modes we developed. In Section 3.1 and Section 3.2 we describe the numerical model and experimental facility used to test the different MI instrumental modes, respectively. In Section 4 we discuss the results of the numerical and experimental investigation. In Section 4.4 we present the cost of the different instrumental modes in terms of the computational load on the onboard computer. In Section 6 we present our conclusions. In Appendix A we describe the characteristics of our experimental facility. In Appendix B we list for repeatability purposes the parameters defining our numerical simulations.

2. Description of MI Instrumental Modes

MI experiments are used to identify in situ the plasma density and electron temperature by, first, perturbing the plasma using a set of emitting antennas in a frequency range encompassing the electron plasma frequency and, second, retrieving the electric fluctuations in the plasma by means of a set of receiving antennas. The emission signal and the data treatment technique to be applied to the retrieved fluctuations depend on the chosen instrumental mode.

To improve the time resolution of MI measurements, we propose (for the first time) two new MI instrumental modes: the chirp mode and the multi-spectral mode. Such new modes are validated by testing their measurements against those of the nominal instrumental mode (Trotignon et al., 2007) which we call here frequency sweep mode and use as a reference.

In the following sections, we recall the experimental procedure of the frequency sweep mode and describe the new chirp and multi-spectral modes.

2.1. Description of the Frequency Sweep Mode

The frequency sweep mode is the state-of-the-art of MI experimental procedures and it is typically used in space applications as the MI nominal instrumental mode. Using this mode, MI spectra are built in four steps.

First, the plasma is excited by a sequence of elementary sinusoidal signals from the emitting electric antennas. The electric potential imposed at the antennas for the emission of the $i-th$ elementary signal reads:

$$V_{sw,i} = A\ \sin(2\pi f_i t) \quad (t_i < t < t_i + N/f_i, N = 20, 0 \le i \le j-1) \tag{1}$$

where $V_{sw,i}$ is the electric potential, A is the (fixed) emission amplitude, $f_i = f_{\min}(1+\Delta)^i, i = 0, \ldots, j-1$ is the frequency, $T_i = N/f_i$ is the emission duration, t_i is the beginning time of the emission of the $i-th$ frequency, $f_{\min}$ is the lower scanned frequency, $j = 1 + \log(f_{\max}/f_{\min})/\log(1+\Delta)$ is the number of emitted frequencies, Δ is the relative frequency resolution of the measurement and N is the amount of emitted oscillations per frequency (repetitions). To mimic typical MI space applications (e.g., the COMPLIMENT instrument onboard Comet Interceptor) we choose $\Delta = 0.05$.

Second, simultaneously to the emission process, the electric fluctuations generated in the plasma are measured by the receiving antennas.

Third, Discrete Fourier Transforms (DFTs) of the received electric signals are computed around the emitted frequencies. In particular, for the received electric fluctuations corresponding to the $i-th$ elementary signal, we compute the DFT at frequency f_i. This is done for all emitted frequencies.

Fourth, from the DFT components, we build spectra in phase and amplitude. MI spectra are then obtained by normalizing such spectra to the corresponding reference spectral response for the instrument. This reference response is identified by spectra obtained either in vacuum or in low density plasmas, such as weakly active solar wind conditions, following the procedure described above.

The frequency range $(f_{\min}, f_{\max})$ investigated with MI measurements is chosen in function of the probed plasma environment and therefore changes between different missions with different targets.

In past and current MI experimental space applications (e.g., Rosetta/RPC-MIP, BepiColombo/RPWI/AM2P, JUICE/PWI/MIME), the emission duration is fixed whatever the emitted frequency. As a consequence, the amounts of repetitions N is dependent on the emitted frequency. Overall, for such applications we find repetitions ranging between $N = 8$ and $N = 1{,}000$. In the case of DFP-COMPLIMENT onboard the future Comet Interceptor mission, instead, $N = 20$ has been chosen for all frequencies. As a consequence, different frequencies will correspond to different emission durations. In our investigation, we choose to mimic DFP-COMPLIMENT and fix the amount of repetitions to $N = 20$. Therefore, the total duration of the frequency sweep measurements investigated in our study corresponds to $T_{i,sw} = N \sum_{i=0}^{j-1} 1/f_i$.

2.2. Description of the Chirp Mode

The chirp mode is a new MI instrumental mode designed to minimize the time required by MI experiments to perform one single measurement. This is achieved by following the same procedure used for the frequency sweep mode, but by emitting each elementary signal for only one repetition (i.e., $N = 1$). For this mode, MI spectra are built from the components of the Fast Fourier Transform (FFT) of the whole received signal. Contrary to the frequency sweep mode that treats each frequency sequentially, the chirp mode treats all frequencies at once. When required, we use a Hann window to reduce the spectral leakage related to the non-periodicity of the electric potential retrieved by the receiving antennas. The need for the windowing of this signal is discussed in Section 4.3.

The oscillating electric potential used to polarize MI electrodes for the chirp emission reads:

$$V_{ch} = A \ \sin(2\pi f_i t) \quad (t_i < t < t_i + 1/f_i, 0 \le i \le j-1) \tag{2}$$

Hence, using this chirp mode, the MI measurement duration is reduced by about N times with respect to a corresponding frequency sweep mode measurement. The total duration of one chirp measurement is $T_{t,ch} = \sum_{i=0}^{j-1} 1/f_i$.

2.3. Description of the Multi-Spectral Mode

Similarly to the chirp mode, the multi-spectral mode is also a new instrumental mode devised to minimize the duration of MI measurements. The difference from the frequency sweep mode is that multiple elementary signals are emitted simultaneously. This choice reduces the measurement duration, but at the same time affects the amplitude of the emitted signals. Indeed, the instrument electronics can deliver to the electric antennas a signal with given maximum amplitude and, therefore, the superposition of different elementary signals has to respect this constraint. All in all, the choice of how many signals should be emitted simultaneously is the result of a trade-off between short measurement duration and strong enough received electric signals to ensure a satisfactory Signal-to-Noise Ratio. In our investigation we choose to emit simultaneously nine different elementary signals each with amplitude $A/9$. For the $i-th$ emission, the electric potential imposed at the antennas reads:

$$V_{ms,i} = \sum_{k=1}^{9} \frac{A}{9} \sin(2\pi f_{k,i} t) \quad (t_i < t < t_i + N/f_{0,i}, N = 20, 0 \le i \le j-1) \tag{3}$$

where $V_{ms,i}$ is the electric potential, $f_{0,i}$, …., $f_{8,i}$ are the frequencies emitted simultaneously, and $T_i = N/f_{0,i}$ is the $i-th$ emission duration with $N = 20$ oscillations. Similarly to the frequency sweep mode procedure, the electric fluctuations generated in the plasma are retrieved simultaneously to each $i-th$ emission of the signal $V_{ms,i}$. Then, MI spectra are built by computing DFTs of those fluctuations for the corresponding emitted frequencies $f_{k,i}$ with $k = 0, .., 8$.

Depending on which frequencies we emit simultaneously, we obtain different MI emission durations. The minimum duration is obtained by grouping the lower frequencies in the same $i-th$ emission. But, if the simultaneously emitted signals have frequencies too close to each other, they can interfere and generate beats. In such case, the energy injected in the plasma at the emitted frequencies would shift to other frequencies and the measurements would be affected. In order to minimize this effect, we need to impose that the minimum difference between the frequencies we emit simultaneously is larger than some multiples of the frequency resolution of our spectral analysis. For each $i-th$ emission, such resolution corresponds to the inverse of the emission duration (i.e., $\Delta_{A,i} = f_{1,i}/N$). Considering (a) a measurement resolution of $\Delta = 0.05$ and (b) $N = 20$ for the lower frequencies

of the same $i-th$ emission, we find negligible interferences if the frequencies emitted simultaneously are spaced by at least $y=5$ other frequencies along the frequency range of interest. This means that the frequencies that are part of the same $i-th$ emission are different by at least a factor $(1+\Delta)^5$. The value of y is found empirically, by imposing that the DFT of $V_{ms,i}$ gives for the frequencies $f_{k,i}$ the amplitude $A/9$ with a precision of 2%.

For completeness, we give an empirical rule to compute the different sets of frequencies emitted simultaneously. For the $i-th$ emission, we emit the frequencies $f_{k,i}=f_{\min}(1+\Delta)^{y\ k+p_1+p_2}$ with $k=0,\ldots,8$ their index, $p_1=i \bmod y$ and $p_2=(9\cdot y)\cdot(i \operatorname{div} y)$ (where div represents the Euclidean division and mod the remainder of the Euclidean division). Note that one multi-spectral measurement is composed of $p_3=[(j-1)\bmod(9\cdot y)+1]\cdot y$ simultaneous emissions and receptions. Let us consider the case where the multi-spectral measurement scans $j=81$ frequencies with resolution $\Delta=0.05$, $N=20$ (i.e., $y=5$) and a maximum of 9 frequencies emitted simultaneously. Then, the measurement is composed of $p_3=10$ emissions and the frequencies emitted simultaneously are:

$$
\begin{aligned}
&f_{0,0}=f_0, f_{1,0}=f_5, f_{2,0}=f_{10}, f_{3,0}=f_{15}, f_{4,0}=f_{20}, f_{5,0}=f_{25}, f_{6,0}=f_{30}, f_{7,0}=f_{35}, f_{8,0}=f_{40}\\
&f_{0,1}=f_1, f_{1,1}=f_6, f_{2,1}=f_{11}, f_{3,1}=f_{16}, f_{4,1}=f_{21}, f_{5,1}=f_{26}, f_{6,1}=f_{31}, f_{7,1}=f_{36}, f_{8,1}=f_{41}\\
&f_{0,2}=f_2, f_{1,2}=f_7, f_{2,2}=f_{12}, f_{3,2}=f_{17}, f_{4,2}=f_{22}, f_{5,2}=f_{27}, f_{6,2}=f_{32}, f_{7,2}=f_{37}, f_{8,2}=f_{42}\\
&f_{0,3}=f_3, f_{1,3}=f_8, f_{2,3}=f_{13}, f_{3,3}=f_{18}, f_{4,3}=f_{23}, f_{5,3}=f_{28}, f_{6,3}=f_{33}, f_{7,3}=f_{38}, f_{8,3}=f_{43}\\
&f_{0,4}=f_4, f_{1,4}=f_9, f_{2,4}=f_{14}, f_{3,4}=f_{19}, f_{4,4}=f_{24}, f_{5,4}=f_{29}, f_{6,4}=f_{34}, f_{7,4}=f_{39}, f_{8,4}=f_{44}\\
&f_{0,5}=f_{45}, f_{1,5}=f_{50}, f_{2,5}=f_{55}, f_{3,5}=f_{60}, f_{4,5}=f_{65}, f_{5,5}=f_{70}, f_{6,5}=f_{75}, f_{7,5}=f_{80}\\
&f_{0,6}=f_{46}, f_{1,6}=f_{51}, f_{2,6}=f_{56}, f_{3,6}=f_{61}, f_{4,6}=f_{66}, f_{5,6}=f_{71}, f_{6,6}=f_{76}, f_{7,6}=f_{81}\\
&f_{0,7}=f_{47}, f_{1,7}=f_{52}, f_{2,7}=f_{57}, f_{3,7}=f_{62}, f_{4,7}=f_{67}, f_{5,7}=f_{72}, f_{6,7}=f_{77}\\
&f_{0,8}=f_{48}, f_{1,8}=f_{53}, f_{2,8}=f_{58}, f_{3,8}=f_{63}, f_{4,8}=f_{68}, f_{5,8}=f_{73}, f_{6,8}=f_{78}\\
&f_{0,9}=f_{49}, f_{1,9}=f_{54}, f_{2,9}=f_{59}, f_{3,9}=f_{64}, f_{4,9}=f_{69}, f_{5,9}=f_{74}, f_{6,9}=f_{79}
\end{aligned}
\tag{4}
$$

The total duration of one multi-spectral measurement is $T_{t,ms}=N\sum_{i=0}^{p_3-1}1/f_{0,i}$.

3. Methods

In this section, we describe the numerical model and the experimental facility we used to test and characterize the chirp and multi-spectral modes against the reference frequency sweep mode.

3.1. Full-Kinetic Electrostatic 1D-1V Vlasov-Poisson Simulation Model

We investigate numerically the new MI instrumental modes by performing numerical simulations of an unmagnetized, collisionless, homogeneous plasma perturbed by MI emitting electric antennas. For this purpose, we use a 1D-1V full kinetic electrostatic model (Bucciantini et al., 2022; Henri et al., 2010) based on the solution of the Vlasov-Poisson system (following the integration scheme of Mangeney et al. (2002)) to simulate the evolution in time and space of the electron distribution function ($f_e(t,x,v_e)$, where t is the time, x the position and v is the velocity) of a numerical plasma box. In particular, the electron distribution functions at different positions in the numerical box are evolved in time by using the Vlasov equation:

$$
\frac{\partial f_e(x,t,v_e)}{\partial t}+v_e\frac{\partial}{\partial x}f_e(x,t,v_e)-\frac{e}{m_e}E\frac{\partial}{\partial v_e}f_e(x,t,v_e)=0 \tag{5}
$$

where e is the electron charge, m_e is the electron mass, and E is the electric field of the plasma box. Such electric field is computed self-consistently using the Poisson equation:

$$
\frac{\partial E}{\partial x}=e\frac{n_i-n_e(x,t)}{\varepsilon_0}+\frac{\rho_{ext}(x,t)}{\varepsilon_0} \tag{6}
$$

where n_i is the fixed homogeneous ion density in the numerical box and ρ_{ext} is an external source term that we use to model MI emitting antennas. For each emitting antenna, the external source term reads:

$$
\rho_{ext}(x,t)=\sigma_0\delta(x)\ \sin(2\pi f t) \tag{7}
$$

where σ_0 is the emission amplitude and f is the emitted frequency. Each MI emitting antenna modeled in 1D as a localized oscillating external electric charge corresponds, in 3D, to a uniformly charged infinite planar grid. Such a grid is assumed transparent, so that the currents collected at its surfaces are negligible.

We use periodic boundary conditions in physical space, and we assume that the distribution functions are equal to zero for velocities outside the chosen velocity space range (e.g., $f_e(x, |v_e| > v_{\max\ e}, t) = 0$). The periodic boundary conditions require a spatially periodic electric field and electric potential in the box. But the plasma located on the two sides of each emitting (infinite planar grid) antenna is perturbed with electric fields of opposite signs. It follows that the spatial periodicity of the system cannot be ensured by the use of only one emitting antenna. Therefore, we use multiple antennas and arrange them so that their resulting electric field and electric potential are periodic in the box. Practically, we use four emitting antennas: two antennas with positive charge and two antennas with negative charge, equally spaced along the 1D numerical box and ordered as a sequence of negatively-positively-positively-negatively charged antennas. Such configuration mimics a succession of two infinite plate capacitors, where each capacitor is composed of two contiguous antennas with opposite charge. The two capacitors induce in-between their electrodes opposite electric fields, resulting in opposite electric potential variations of the plasma. As a result, our configuration ensures the periodicity of both the electric field and electric potential in the box.

Ions are modeled as a homogeneous neutralizing fixed background of positive charges. This is justified because both the MI antenna emission amplitudes and the MI measurement durations ensure a negligible contribution of the ion dynamics to MI measurements. First, the chosen emission amplitudes (Appendix B) correspond to electric-to-thermal energy ratios well below 0.1. Therefore, the energy injected by the MI antennas in the plasma is small with respect to the kinetic energy of electrons and no non-linear interactions (e.g., wave-wave or wave-particle interactions) are triggered. Second, our numerical simulations are focused on MI measurement durations that are much shorter than ion time scales.

To minimize possible transient effects, the model is initialized by imposing the respect of both the Poisson and Ampère-Maxwell equation at $t = 0$.

For repeatability purposes, we list in Appendix B the parameters defining the numerical simulations discussed in our investigation.

3.2. PEPSO: Plasma Chamber Experimental Facility

In this section, we describe the plasma chamber testing facility used to validate the diagnostic performance of MI instrumental modes. This testing facility was developed in the framework of the PEPSO project (Plasma Environment Platform for Satellite tests in Orléans) at the LPC2E (CNRS, Orléans, France) space laboratory. It is composed of a vacuum chamber, a pumping system, a plasma source, a magnetic field control system, and various diagnostics devices.

The vacuum chamber is a cylindrical chamber in AlSI304 L alloy, measuring 1 m in diameter and 1.8 m in length.

The pumping system, composed of a primary pump (Pfeiffer/ACP40) and a secondary turbo-molecular pump (Pfeiffer/ATH3204M), is used to bring the ambient pressure in the chamber down to 10^{-6} mbar (i.e., about 10^{-4} Pa).

The plasma source is a Kaufman type (Kaufman et al., 1982) electric source, composed of an ionization chamber, a cathode (tungsten) filament, a filtering electric grid, a neutralizing (tungsten) filament and an external solenoid. Inert neutral gas (Argon >99.999%) is injected in the ionization chamber. The cathode filament is heated and electrons are thermionically emitted. The neutral gas flow entering the source is ionized through collisions with these electrons. Positive ions produced by the collisions are accelerated outside the source by the filtering grid while released electrons are kept inside it in order to maintain the ionization process of the gas. Similarly to the cathode, the neutralizing filament outside the source is heated and electrons are thermionically emitted. Such electrons do not remain near the filament but, instead, are attracted by the positive potential of the ion flow. As a result, the electrons join the ion flow and form a globally neutral plasma which drifts along the chamber. The external solenoid is used to modify the magnetic field inside the source in order to constrain the movement of electrons and increase the ionization of the gas. At the middle of the chamber (where we typically place our instrumentation), the injected plasma has a density ranging between 5×10^4 and 4×10^5 cm^{-3} and an electron

Table 1
List of Plasma Density and Electron Temperature Parameters Characterizing the Two Experimental Tests Discussed in Section 4

Test	n_e[cm^{-3}]	T_e[eV]
T_01	53,156 ± 3195	0.47 ± 0.20
T_02	67,970 ± 3485	0.49 ± 0.03

temperature of the order of 0.5 eV. The corresponding Debye length is of the order of 0.008–0.023 m, which is small compared to the size of the vacuum chamber.

Modifications of the neutral gas flow rate and/or settings of the plasma source enable one to control the characteristics of the generated plasma. In the following sections, we illustrate two examples of experimental tests, performed using the two different sets of plasma parameters listed in Table 1. We discuss the stability and the homogeneity of the plasma flow injected in the vacuum chamber, together with its drift velocity, in a dedicated Appendix A.

After the plasma is generated in the chamber, we perform MI measurements using a monopolar electric emitting antenna, a dipolar set of receiving antennas and one electronic card. The two antennas are aluminum spherical antennas (radius of 0.01 m) placed close to the axis of the cylindrical plasma chamber, perpendicular to the plasma flow and at a distance of 0.15 m between each other. The geometric configuration of the antennas in the plasma chamber is represented in Figure 1.

The receiving antenna is connected to an amplifier which increases the received signal amplitude by a factor 8.7 (i.e., 18.79 dB). The electronic card is used to perform MI measurements following the emission/reception procedures described in Section 2 for the different investigated instrumental modes. For this purpose, we choose the Eclypse evaluation board which integrates a Zynq7000 processor (Xilinx), equipped with Digital-to-Analog and Analog-to-Digital converters.

At the position of the electric antennas, the Earth's magnetic field amplitude amounts to 3.8×10^4 nT (i.e., 0.38 G). To this magnetic field corresponds the plasma cyclotron frequency $f_{ce} = 1.1$ MHz, which we note is of the same order as the plasma frequency in the plasma chamber. In this case, Larmor radius is estimated to be 4 cm. If the electron cyclotron frequency is of the same order as the plasma frequency, the Larmor radius is also of the same order as Debye length. Hence, the contribution of Earth's magnetic field to MI spectra is non-negligible.

Figure 1. Plasma chamber. Experimental configuration of the electric antennas used to validate the new MI instrumental modes.

To mimic typical planetary and cometary ionized environments characterized by a low magnetic field, we need to significantly reduce Earth's background magnetic field at the position of MI antennas. For this purpose, we use a magnetic field control system. Such system is composed of three perpendicular pairs of wire coils, each coil is located on one face of a cube, and its diameter is equal to the cube side length, in a configuration similar to three Helmholtz coils (as in Figure 1). By sending currents in the coils, we modify the amplitude of the magnetic field at the antenna location down to about 6% of its ambient value. As a result of such reduction in magnetic field strength, the approximation of an unmagnetized plasma (i.e., $\omega_p/\omega_{ce} \gg 1$) is valid. We note that our numerical model (Section 3.1) is consistent with this unmagnetized plasma experimental setup.

4. Results

In this section, we compare frequency sweep mode measurements to chirp and multi-spectral mode measurements. We obtain MI spectra following the experimental procedures described in Section 2.

This investigation is performed both numerically, using the model described in Section 3.1, and experimentally, using the plasma chamber described in Section 3.2.

4.1. Numerical Investigation

We simulate MI measurements for the frequency range $(0.5f_p, 3.2f_p)$ with frequency resolution $\Delta = 0.05$ ($j = 39$), consistent with the resolution used

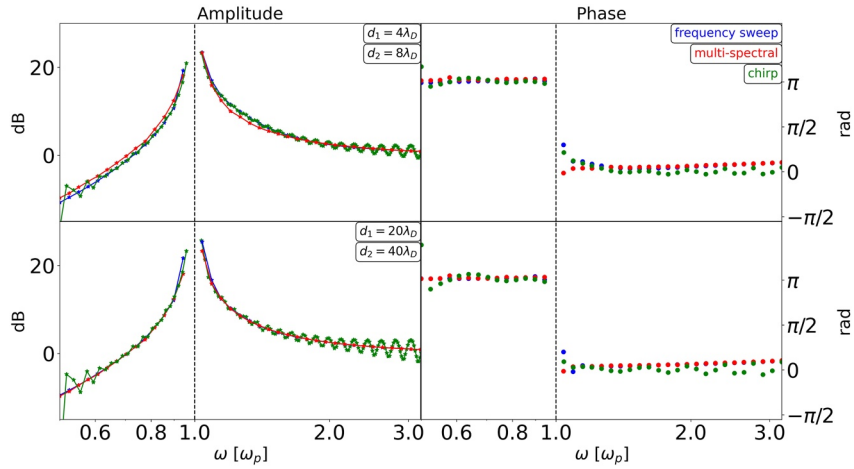

Figure 2. Mutual impedance amplitude and phase spectra (left and right panels, respectively) obtained numerically for the frequency sweep mode (blue line), chirp mode (green line) and multi-spectral mode (red line). Top and bottom panels are obtained for distances $d = 4\ \lambda_D$ and $d = 20\ \lambda_D$, respectively. The black dashed lines indicate the position of the plasma frequency.

by the DFP-COMPLIMENT instrument onboard the Comet Interceptor mission. This resolution corresponds to a relative plasma density uncertainty of $\Delta n_e/n_e = 10\%$, with n_e the plasma density, consistent with space exploration missions needs and requirements.

MI spectra are built from the electric potential difference measured between two receiving antennas, one at distance d and one at 2 d from the emitting antennas. We limit our investigation to distances d ranging from 4 λ_D to 100 λ_D, which corresponds to the typical distance between emitting and receiving antennas for experimental space applications.

Depending on the investigated instrumental mode, we employ either a single or multiple numerical run(s) to simulate one given MI measurement.

First, for the frequency sweep mode (simulations FS_01 to FS_48 in Table B1), instead of using one single run to simulate the emission of a succession of elementary signals, we use several runs to simulate separately the emission of each single signal $V_{sw,i}$. In our case, given the investigated frequency range and frequency resolution, we perform 39 different runs. Since our numerical box is periodic and wave reflections are to be avoided, by doing so we reduce the size of the numerical spatial box and the computational cost of our simulations. This is achieved at the expense of neglecting the coupling between electric fluctuations of the plasma corresponding to the emission of different elementary signals. This approach is justified by the use of small emission amplitudes that ensures the absence of non-linear interactions between plasma perturbations at different frequencies. Second, for the chirp mode (simulation CH_01), the emission process is simulated using one single numerical run. Third, for the multi-spectral mode (simulations MS_01 to MS_06), similarly to the frequency sweep mode case, we simulate separately the emission of each signal $V_{ms,i}$. In our case, given the investigated frequency range and its resolution, we perform six different runs.

Different examples of numerical MI spectra obtained for the frequency sweep (solid blue line), chirp (solid green line) and multi-spectral (solid red line) modes are shown in Figure 2, for distances $d = 4\ \lambda_D$ and $d = 20\ \lambda_D$ (top and bottom panel, respectively). The reference plasma frequency is shown using black vertical dashed lines. These spectra are represented in decibel scale, where the 0 dB corresponds to the electric potential difference obtained in vacuum, using the same normalization as usually performed in the post-treatment of space missions MI spectra.

All spectra exhibit a resonant peak in correspondence to the plasma frequency. This is the signature of MI measurements which enables one to identify, from the frequency location of the resonance at the plasma frequency, the plasma density and, from the shape of the resonance itself, the electron temperature (Bahnsen et al., 1988; Béghin & Debrie, 1972; Décréau et al., 1978; Geiswiller et al., 2001; Gilet et al., 2017; Grard, 1969, 1997; Pottelette et al., 1975; Pottelette & Storey, 1981; Rooy et al., 1972; Storey et al., 1969; Wattieaux et al., 2020).

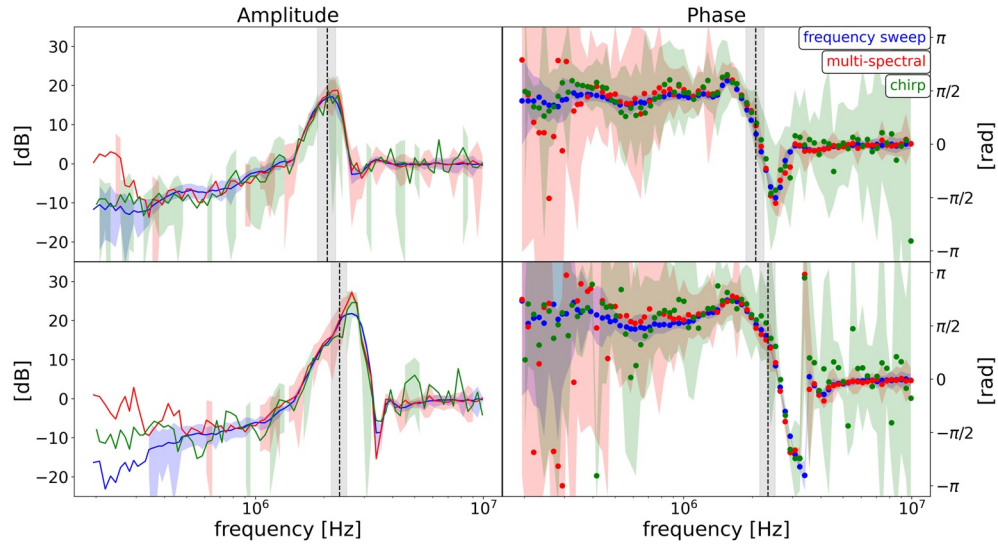

Figure 3. Mutual impedance spectra in amplitude (left column) and phase (right column) obtained experimentally for the frequency sweep mode (blue line), chirp mode (green line) and multi-spectral mode (red line). Each row represents tests performed for a different plasma (plasma densities listed in Table 1, increasing from top to bottom row). The black dashed line indicates the reference plasma frequency obtained from an independent measurement and the gray shaded area the associated uncertainty.

We find that multi-spectral measurements and reference frequency sweep measurements differ at most of 2.5 dB in correspondence to the plasma resonance. We consider such difference negligible because of the order of the typical 1 dB MI instrumental noise found in space applications.

Chirp and frequency sweep measurements have differences of 2.5 dB only for frequencies close to the plasma frequency (i.e., in the range [0.7 ω_p, 1.5 ω_p]). For frequencies far from the plasma frequency (i.e., below 0.7ω_p or above 1.5 ω_p), instead, the discrepancies significantly exceed (i.e., larger than 5 dB) the typical instrumental noise levels.

Since small discrepancies are observed for the resonant signature of the two MI measurements, which is used to derive the plasma density and electron temperature, we conclude that the three instrumental modes should provide identical densities and temperatures.

In the following section, we validate experimentally the new MI instrumental modes by comparing multiple spectra obtained in the plasma chamber.

4.2. Experimental Investigation

We obtain experimental MI spectra within the frequency range (200 kHz, 10 MHz), using the frequency resolution Δ (i.e., $\Delta n_e/n_e = 10\%$) resulting in $j = 81$. For this purpose, we use the MI antennas configuration described in Section 3.2.

Typical examples of experimental MI spectra in amplitude and phase are shown in Figure 3 (left and right panels, respectively). Such spectra are obtained using the frequency sweep (blue line), chirp (green line) and multi-spectral (red line) modes to probe plasmas in the chamber characterized by different plasma densities (increasing from top to bottom panel), with densities listed in Table 1). The spectrum obtained for each mode is the median spectrum computed from a repetition of 11 independent successive measurements. The colored shaded areas represent the uncertainty of the measurements, identified to the standard deviation of each Fourier component derived from the 11 measurements. For the sake of comparison with the other instrumental modes, we only show the Fourier components computed for the emitted frequencies, even for the chirp mode spectrum that is obtained using an FFT.

For frequency ranges encompassing the resonant signature of the spectra, we find both small uncertainties (i.e., a small standard deviation) and identical spectra (both in amplitude and in phase) for the three investigated

instrumental modes. In particular, for such frequency ranges (e.g., for the range 1 MHz to 4 MHz), we find discrepancies up to 2.15 dB (resp. 1.5 dB) in amplitude and 0.57 rad (resp. 0.42 rad) in phase for chirp (resp. multi-spectral) measurements. Larger discrepancies are found, instead, for frequencies outside the resonant regions.

We note that the measurements' uncertainty is larger for the chirp and multi-spectral modes than for the frequency sweep mode. Indeed, the experimental system noise affects the measurements differently, depending on the instrumental mode. Noise affects frequency sweep and multi-spectral measurements when spurious electric oscillations at a given frequency and with sufficiently large amplitude are present in the plasma, while that same frequency is emitted by the instrument. For the multi-spectral mode, the same perturbations experienced by frequency sweep measurements generates a signal-to-noise ratio nine times smaller because the emission amplitude itself is nine times smaller (see Section 2.3). Chirp measurements, instead, are affected by noise when spurious oscillations perturb the probed plasma during the measurement, whenever during the entire measurement and not only when the corresponding frequency is being emitted. As a consequence, noise perturbations are more likely to affect chirp than frequency sweep measurements.

We note that the MI spectra uncertainties found experimentally significantly exceed the typical 1 dB uncertainty expected for MI measurements performed in space. Such uncertainties are due to the vicinity to the MI antennas of the vacuum chamber and plasma source, that affect the measurements with their presence. Smaller uncertainties, of the order of 1 dB for the frequency sweep measurements, are expected in space.

For both our numerical and experiment investigations, we have shown that the MI spectra obtained for the new MI instrumental modes are almost identical to the reference frequency sweep measurements. We have therefore decided to compare directly the different measured spectra, instead of the physical parameters derived from each spectrum. The identification of physical plasma parameters (i.e., the plasma density and electron temperature) from the MI spectra in the case of frequency sweep measurements is out of the scope of this paper, as it has been already described in previous papers (Bahnsen et al., 1988; Béghin, 1995; Béghin & Debrie, 1972; J. Chasseriaux et al., 1972; J. M. Chasseriaux, 1972; J. M. Chasseriaux, 1974; Décréau et al., 1978; Geiswiller et al., 2001; Gilet et al., 2017; Grard, 1997; Pottelette et al., 1975; Pottelette & Storey, 1981; Rooy et al., 1972; Storey et al., 1969; Wattieaux, G. et al., 2019). Our current study shows that this instrumental theory can directly be used to also provide plasma parameters from MI spectra obtained from both the multi-spectral and the chirp instrumental modes.

4.3. Difference Between Numerical and Experimental Chirp Measurements

In the previous section, we have compared the new MI chirp and multi-spectral measurements to the nominal frequency sweep measurements in order to assess the impact of short emission durations on the MI plasma diagnostic. We have found that chirp and multi-spectral measurements are very similar (see Section 4) to frequency sweep measurements. To achieve such results, we had to introduce for the numerical tests of the chirp mode a window function (i.e., Hann) in the procedure. In this section, we explain why such windowing is needed for the numerical investigation of the chirp mode while it is not for its experimental counterpart.

Examples of emitted (black line) and received (green line) electric potential signals corresponding to both numerical (top panel) or experimental (bottom panel) chirp measurements are shown in Figure 4.

Both in simulations (top panel) and in the plasma chamber (bottom panel), the emission process triggers oscillations of the plasma at the emitted frequencies. For emitted signals at frequencies far from the resonant frequency of the system (i.e., the plasma frequency) the plasma reacts with small oscillation amplitudes at those frequencies, as expected. In particular, the high frequencies emitted at time 220 ω_p^{-1} (top panel) and time 105 μs (bottom panel) correspond to received electric potential oscillations associated to negligible amplitudes. This is consistent with the strong Landau damping expected at these frequencies, so that the signal cannot propagate for long. For emitted signals at frequencies close to the plasma frequency, the amplitude of the oscillations increases as the plasma resonates, as expected. This is observed at time 150 ω_p^{-1} (top panel) and time 97 μs (bottom panel). However, after the resonance is triggered, two different features are observed for the numerical and experimental investigation. Numerical tests suggest that oscillations at the plasma frequency do not disappear from the received electric signal even after the emission process stops (i.e., after time $t = 225\ \omega_p^{-1}$, top panel). This is consistent with the fact that (a) the Landau damping of Langmuir waves is negligible at the plasma frequency and (b) the group velocity of Langmuir waves vanishes at the plasma frequency. Therefore, the oscillation at the plasma

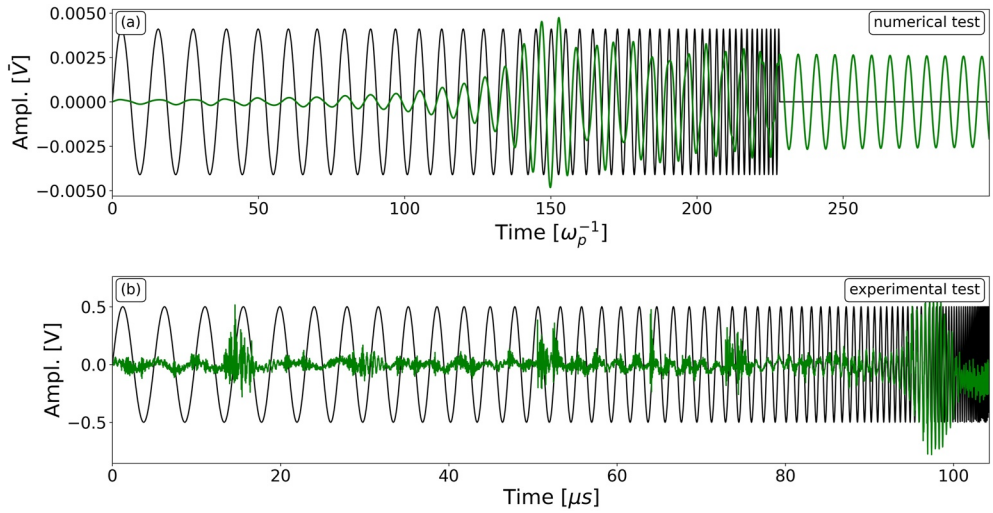

Figure 4. Example of numerical and experimental chirp measurements. The amplitude of emitted (black line) and received (green line) electric signals is represented in function of time. Panel (a) (resp. Panel (b)) represents the signals obtained numerically (resp. experimentally).

frequency is indeed expected to remain observable at the instrument location. Experimental tests, instead, show that oscillations at the plasma frequency are not measured for long after they are triggered. In particular, between 98 and 100 μs in Figure 4 (bottom panel) the plasma does not oscillate at the resonant frequency registered at 97 μs. Instead, it is synchronized with the emission. Note that, in this analysis, we neglect the plasma fluctuations at high frequencies (e.g., 105 μs) and we only focus on plasma fluctuations that oscillate at the resonant frequency (i.e., at about 97 μs). The reason behind such choice is that both the plasma density and the electron temperature are derived from the resonance of MI spectra. Hence, the resonance is the only signature of MI measurements that is of interest in this investigation. Since the chirp analysis is performed on the electric potential oscillations measured synchronously to the emission, the total analyzed signal is quasi-periodic only in the experimental case and not in the numerical case. Some apodization procedure is therefore required in the numerical case. For consistency with the frequency sweep and multi-spectral mode, before building the chirp spectra from Figure 2 we used a Hann window to filter the electric oscillations retrieved by the chirp reception.Let us now investigate the possible reasons for such different behavior observed with numerical and experimental chirp measurements.

First, the numerical model assumes a collisionless plasma. Is the plasma in the chamber collisional in the regions close to the antennas? If that is the case, the resonant plasma oscillations would be damped by electron-neutral collisions with a damping rate corresponding to the electron-neutral collision frequency. This could explain why they are not observed for as long as our numerical investigation suggests.

We have computed the electron-neutral mean-free-path in the chamber to assess if the generated plasma is collisional. We obtain $l_{el} \simeq 500$ m, which is much larger than both the distance between the MI electric sensors (i.e., 0.3 m) and the Debye length (i.e., 0.008–0.023 m). Such mean free path of electron-neutral (Argon) collisions ($l_{el} = 1/(\sigma_{el} n_{Ar})$ was computed using the ambient pressure ($P_a \simeq 2.5 \times 10^{-3}\ Pa$) measured in the chamber during the experimental tests, the ambient temperature ($T \simeq 300$ K), the neutral Argon density $n_{Ar} = P_d/(k_B T)$, the elastic electron-neutral collision cross-section ($\sigma_{el} = 3 \times 10^{-21}$ m^2 (Gargioni & Grosswendt, 2008)) and the thermal velocity of electrons ($v_{the} = 300$ km/s). Therefore, the plasma in the chamber is confirmed to be collisionless, and collisions cannot explain the disappearance of the resonant oscillations from the received signal in the experimental tests.

Second, the numerical model assumes a non-drifting plasma while the plasma in the chamber is actually drifting from the plasma source, at velocity v_D of about (1–15) km/s (Appendix A). Is this drift velocity large enough to enable the oscillating plasma to drift away from MI antennas over a characteristic time that is negligible compared to chirp measurement durations? For convenience, let us assume that the plasma drifts along the chamber with constant velocity $v_D = 15$ km/s. Since the chamber measures 1.8 m, over a characteristic travel time $t_{tr.} = 1.8$ m/$v_D = 120$ μs the plasma travels along its whole length, from the plasma source to the back wall of the chamber.

Considering that MI antennas are placed in the middle of the chamber, the plasma drifts away from them in about $t_{tr.}/2 = 60$ µs. This characteristic time is not negligible with respect to chirp measurement durations, which in our investigation amounts to about 100 µs. Therefore, the drift velocity in the chamber is not fast enough to explain the disappearance of resonant oscillations from the experimental chirp measurements.

We note that the magnetic field compensation system reduces the magnetic field amplitude at the position of the plasma probed by the antennas (Section 3.2). Therefore, the gyration of particles can be neglected in this study and the magnetic field cannot explain the difference between numerical and experimental measurements.

Since, for the experimental tests, our two hypotheses can not explain the disappearance of plasma frequency oscillations from the retrieved electric potential measurements, this discussion remains open. To date, we have no robust explanation for this observed discrepancy between numerical and experimental chirp measurements. Since it seems to be related to the presence of the testing facility and its effects on MI measurements, we leave the resolution of this discrepancy to future space measurements using the newly designed chirp mode.

4.4. Computing Resources Evaluation for Frequency Sweep, Chirp and Multi-Spectral Measurements

In the previous sections, we have compared, using numerical and experimental approaches, MI measurements performed following the frequency sweep, chirp and multi-spectral procedures. In this section, we take a practical (instrumental) point of view and compare the amount of onboard computations that would be required for these three modes. The onboard calculator is identified to be the critical function, to discriminate the three modes in terms of electric power consumption. For this reason, we quantify and compare the amount of arithmetical operations needed by each mode to produce a single MI measurement. This is directly proportional to the power required by the onboard computer to perform the measurement. We note that the purpose of this section is only to provide a reference value of the computing resources (thus the power consumption) of the three MI instrumental modes. More precise estimates require the exact definition of the algorithms used to build the MI spectra, which depend on the particular space application of interest and are out of the scope of this paper.

We assume that the received signal is sampled using the same sampling frequency f_s for the three modes. Such frequency is chosen equal to the Nyquist frequency of the investigated frequency range (i.e., $f_s = 2\,f_{\max}$).

For the frequency sweep mode, each frequency f_i with $i = 0, \ldots j-1$ is emitted for the emission duration $T_i = N/f_i$ with $N = 20$. The electric fluctuations generated in the plasma by the emission of frequency f_i are retrieved by means of the receiving antennas and converted by the Analog-to-Digital Converter (ADC) to a digital signal composed of $T_i f_s$ points. The Fourier component of f_i is computed from this digital signal using a DFT technique, resulting in $T_i f_s$ multiplications. The total amount of multiplications performed by the onboard computer to produce one frequency sweep measurement is obtained as the sum of the contributions of all the emitted frequencies, corresponding to $\sum_{i=0}^{j-1} T_i f_s = N f_s \sum_{i=0}^{j-1} 1/f_i$.

For the chirp mode, each frequency f_i is emitted for the duration $T_i = 1/f_i$. The corresponding electric fluctuations triggered in the plasma are retrieved by the receiving antennas and converted to a signal composed of $f_s \sum_{i=0}^{j-1} T_i$ points. Since for this mode we use the FFT technique to build the spectra, the required amount of multiplications scales as $x \log_2(x)$, with x the amount of points in the received signal. Therefore, the amount of onboard computations expected for the chirp mode is $\left(f_s \sum_{i=0}^{j-1} T_i\right)\log_2\left(f_s \sum_{i=0}^{j-1} T_i\right) = \left(f_s \sum_{i=0}^{j-1} 1/f_i\right)\log_2\left(f_s \sum_{i=0}^{j-1} 1/f_i\right)$.

For the multi-spectral mode, frequencies emitted simultaneously have the same emission duration. Considering the total amount of emissions p needed to perform one measurement, for the i-th emission the frequencies $f_{k,i} = f_{\min}(1+\Delta)^{y\ \ k+p_1+p_2}$ (with $k = 0, \ldots, 8$) are emitted for the duration $T_i = N/f_{0,i}$ with $N = 20$. For those frequencies, the received electric fluctuations are converted to a signal of $T_i f_s$ points and the Fourier components are computed using DFTs. As a result, for each of those frequencies the onboard computer executes $T_i f_s$ multiplications. We note that only the frequencies $f_{0,i}$ are emitted for the same duration in the case of both multi-spectral and frequency sweep measurements. All other frequencies have longer durations in the multi-spectral case. Therefore, multi-spectral measurements require more onboard computations than frequency sweep measurements. The total amount of multiplications required to perform one measurement using this technique is $\sum_{i=0}^{p-1} 9 T_i f_s = 9 f_s \sum_{i=0}^{p-1} 1/f_i$, with $p = j$ div 9 if the amount of emitted frequencies (j) is a multiple of 9 (i.e., the amount of simultaneously emitted frequencies), $p = j$ div $9 + j$ mod 9 if not.

To compare the three instrumental modes in terms of duration and computing resources, we consider a practical case where the frequency range of interest is (10 kHz, $f_{\max}$), and we compute both the measurement duration and

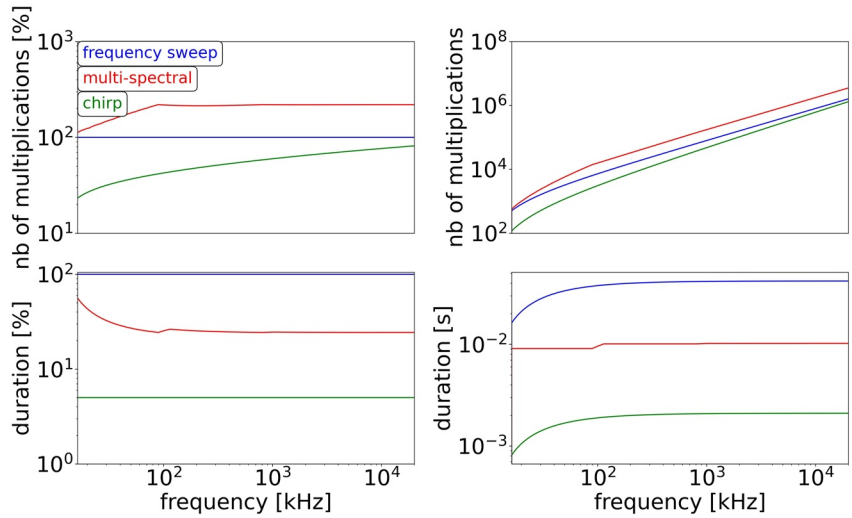

Figure 5. Comparison between software occupation (costs) and sensors occupation time (measurement duration) of the chirp (green lines) and multi-spectral (red lines) modes with respect to the frequency sweep mode (dashed blue line) which is used as reference. Top panels: cost of one mutual impedance measurement in terms of number of multiplications performed by the onboard computer to build one spectrum. The cost is represented in function of the maximum emitted frequency, considering a minimum investigated frequency of 10 kHz and a frequency resolution $\Delta = 0.05$. Bottom panels: MI measurement duration corresponding to the costs of top panel. Left panels illustrate the cost and duration of the three modes normalized to the corresponding frequency sweep curves.

the associated amount of computations as a function of the upper frequency range f_{max}. This is performed with same fixed resolution $\Delta = 0.05$. We show in Figure 5 the cost profile (top panels) and measurement duration (bottom panels) of the new MI instrumental modes in function of the maximum emitted frequency, computed as described above. Costs and duration are illustrated for the chirp (green line) and multi-spectral (red line) modes with respect to the reference cost and duration of the frequency sweep mode (blue dashed line). Both left and right panels represent the same cost and duration curves for the three MI instrumental modes. But, to better highlight the difference of chirp and multi-spectral performances with respect to the frequency sweep mode, the left panels are normalized to the frequency sweep performances.

In Table 2, we list the costs and measurement durations for the frequency sweep, chirp and multi-spectral measurements considering a fixed frequency range (10 kHz, 20 MHz) that is a typical range for ionospheric MI space applications.

Figure 5 and Table 2 show that multi-spectral measurements are up to 4 times faster than frequency sweep measurements, but they require at least twice the amount of operations (i.e., more multiplications) to be performed by the onboard computer. Chirp measurements, instead, are found to be both up to 20 times faster and less demanding (20% less) than frequency sweep and multi-spectral measurements.

Table 2
Comparison of Cost and Duration of the Three Investigated MI Instrumental Modes Considering the Frequency Range (10 kHz, 20 MHz) and the Frequency Resolution $\Delta = 0.05$

Mode	Cost [# of multiplications]	Duration [s]
Frequency sweep	1 6,15 ,868	0.042
Multi-spectral	3 5,41 ,191	0.010
Chirp	1 3,17 ,090	0.002

5. Distinction Between Numerical and Experimental Investigations

In the previous sections, we investigated new MI instrumental modes both numerically and experimentally. For this purpose, we obtained numerical (Figure 2) and experimental (Figure 3) spectra for the frequency sweep, multi-spectral and chirp modes. By comparing such spectra, we note significant differences between theoretical and experimental measurements. Such differences are expected, since the conditions simulated by our numerical model differ considerably from the conditions characterizing our experimental tests.

First, our numerical simulations use periodic boundary conditions in space, while our experimental tests are confined by the plasma chamber. Separate numerical tests performed using the DSCD numerical code (Geiswiller et al., 2001; Wattieaux, G. et al., 2019) show that the presence of the conductive plasma chamber near the MI antennas significantly impacts the measurements.

Second, numerical tests simulate MI measurements in the presence of a steady homogeneous plasma while the plasma within the chamber is an inhomogeneous (Appendix A) drifting (Section 4.3) plasma.

Third, numerical tests assume point emitting antennas as source of the MI emission, while for the experimental tests we use finite size antennas, not negligible with respect to the characteristic length (i.e., Debye length) of the plasma (Section 3.2).

We remind that the goal of our numerical investigation is to enable a comparison of the three MI instrumental modes in a simplified 1D symmetric homogeneous configuration, that aims at providing a physical understanding of the plasma response to MI measurements. Our experimental results, instead, are obtained from a realistic laboratory plasma and, therefore, are directly representative of MI measurements performed in space.

6. Discussion and Conclusions

In order to improve the time resolution of MI experiments, we have defined two new MI instrumental modes called the chirp (Section 2.2) and the multi-spectral modes (Section 2.3). These modes will have a direct application to all the missions where antenna sharing between MI experiments and different experiments occurs, for example, to answer the need for mass and volume minimization onboard nanosatellites. Such new modes are compared numerically and experimentally to the nominal MI instrumental mode, called frequency sweep mode (Section 2.1).

On the one hand, from a plasma diagnostic point of view, we find in our numerical model that chirp and multi-spectral measurements reproduce frequency sweep measurements with negligible amplitude and phase differences. We confirm the results of our model experimentally, as we find that the differences between chirp or multi-spectral measurements and frequency sweep measurements are negligible (i.e., of the order of noise level) for frequencies close to the plasma frequency. Plasma density and electron temperature are directly identified from the analysis of the resonant signature of the spectra, we therefore conclude that these new chirp and multi-spectral modes will have diagnostic performances identical to those of the (reference) frequency sweep mode.

On the other hand, from an instrumental point of view, we focused on both the onboard computation needs, associated to the instrument power consumption, and the time duration of the measurements, associated to the electric sensor occupation.

First, we have shown that multi-spectral measurements require a significantly larger amount of onboard computations (up to 220%) while chirp measurements are significantly less demanding (about 81%) than frequency sweep measurements. The instrument energy consumption strongly depends on the onboard computer energy consumption itself, which is directly related to the amount of onboard computation operations to be performed.

Second, we have shown that both multi-spectral and chirp modes enable to significantly reduce the sensor occupation with respect to the reference frequency sweep mode. Under realistic instrumental assumptions, when performing one single measurement, the multi-spectral mode decreases the antenna occupation by a factor of 5, while the chirp mode decreases it by a factor 20. This means that the time resolution of MI measurements of plasma density and electron temperature will significantly improve (respectively by a factor of 5 or 20) with these new modes.

The associated smaller measurement durations come at the cost of lower signal-to-noise ratios, especially far from the resonance. The newly designed modes should therefore be preferred to the standard frequency sweep mode in cold, dense plasma (i.e., plasmas characterized by a Debye length much smaller than the emitter-receiver distance), where the signal-to-noise ratios of MI measurements is high. However, we warn that the additional noise introduced by these new modes might affect both the electron density and temper-

ature diagnostic performance when the signal-to-noise ratios of MI measurements is low, for example, in low density and/or high temperature plasmas where the Debye length is of the order of the emitter-receiver distance. The MI electron density and temperature diagnostic performance using these new modes might also be affected in the case of multiple electron populations. Past studies (Gilet et al., 2017; Wattieaux et al., 2020) showed that multiple peaks can be found in the resonant signature of MI spectra for plasmas with multiple electron populations. If the spectral noise is significant, single MI measurements with spurious noisy maxima might then be mistaken as a signature of multiple electron populations. If such situations appear, a mitigation solution is to make use of the higher time resolution obtained with these new modes to acquire more measurements, and therefore more statistics to disentangle noise from signal. The modeling of MI spectra in the presence of non-Maxwellian electron distribution functions has been performed successfully in the past (Gilet et al., 2017; Gilet et al., 2019; Wattieaux et al., 2019) for the frequency sweep mode, and our study suggests that the MI spectra will remain unchanged with the newly designed chirp and multi-spectral modes. However, the diagnostic performance of the newly designed chirp and multi-spectral modes in non-Maxwellian plasmas remains out of the scope of this present study and is left for future investigations.

The chirp mode enables to both decrease instrument power consumption, while increasing time resolution and/or reducing at the same time the occupation of a shared sensor, with diagnostic performance almost identical to those obtained with the MI modes used in past space missions. Therefore, all things considered, we conclude that the chirp mode would be the MI instrumental mode to be favored in future space missions.

Appendix A: Properties of the Plasma Generated in the Testing Facility of LPC2E

In this section, we describe the properties of the plasma generated in the testing facility of LPC2E.

Prior to performing our experimental tests, the properties of the plasma injected in the LPC2E vacuum chamber have been investigated with characterization tests. Hereafter, we discuss (a) the stability and (b) the dependency of the plasma parameters on the axial and radial position of the instruments in the chamber. Then, we (c) give the range of drifting velocities found for the plasma inside the chamber.

For these purposes, we use two Langmuir Probes to measure the plasma density and electron temperature inside the chamber. The probes have spherical tips and the sensor's diameter is 0.05 m. The first probe has a fixed boom supporting the sensor and is placed on the axis of the chamber, at about 1.3 m from the source. The second probe has the sensor attached to a flexible support and is installed on a moving device at about 1 m from the plasma source. The moving device is used to shift and rotate the sensor, therefore enabling measurements at different positions in the chamber for the same plasma flow.

The stability of the plasma is investigated by monitoring its properties while modifying them. This is achieved by performing Langmuir Probe measurements right after the electric settings of the plasma source have been modified. The measurements show that, initially, the plasma parameters undergo significant variations. Then, after a given delay, the plasma flow reaches steady state conditions and the parameters become almost fixed. From that instant on, the plasma is stable and MI experiments can be performed. Our tests show that the plasma is stable after a delay of about 30 s. Afterward, the plasma parameters fluctuate around a given value with variations of the order of 2%. As such variations are lower than the typical resolution of MI measurements, it is acceptable to ignore these fluctuations.

The homogeneity of the plasma is investigated by performing Langmuir Probe measurements at different spatial positions in the chamber. This is done by translating and rotating the second Langmuir probe, while keeping the plasma stable. These measurements show the presence of plasma density and electron temperature inhomogeneities in the chamber. In particular, the density (resp. temperature) decreases by a factor 10 (resp. 5) along 46 cm. For a fixed distance from the plasma source, the plasma density is found to be quasi-homogeneous. Therefore, by placing the MI antennas at a fixed distance from the plasma source, the effects of plasma inhomogeneities on MI measurement are neglected in our analysis.

The plasma is generated and injected in the chamber by a Kaufman (Kaufman et al., 1982) electric source which, first, ionizes the inlet neutral Argon gas, second, accelerates with a given electric field its positive ion particles

and, third, neutralizes the flow of ions. It results that the plasma injected in the chamber drifts with a certain drift velocity. Hereafter, we describe the two approaches we used to estimate such velocity.

First, we identify the drift velocity from the electrostatic acceleration of the positive Argon ions at the plasma source. As a first (simplified) estimate, we find that the ions (thus the plasma) drifts in the chamber with drift velocity $v_{D,1} \simeq 15$ km/s, considering the accelerating potential $V_A = 20$ V and the positive Argon ion (Ar^+) mass $m_{Ar} = 3.01 \times 10^{-26}$ kg.

Second, we derive the drift velocity of the plasma flow from Langmuir Probe measurements. To do so, we focus on the ion saturation part of the I-V curve and assume that (i) the ion thermal velocity is negligible with respect to the drift velocity and (ii) the plasma in the chamber is quasi-neutral (i.e., $n_i = n_e$, with n_e the electron density measured by the Langmuir Probe). Then, following the procedure described in Odelstad et al. (2018) (Equation 7), we identify the ion drift velocity from the slope of the ion current. Such relation reads:

$$\frac{\partial I}{\partial V} = \frac{Aq^2 n_i}{2m_i} \frac{\sqrt{(8k_B T_i)/(\pi m_i) + v_D^2}}{(2k_B T_i)/(m_i) + v_D^2} \tag{A1}$$

where I is the ion saturation current, V is the electric potential, $A = 4\pi r^2$ is the surface of the Langmuir Probe, $q = e$ and $m_i = m_{Ar}$ are the charge and mass of the Ar^+ and T_i is the ion temperature. By fitting the equation above to different Langmuir probe data, we find drift velocities in the range $v_{D,2} = 1$–12.5 km/s.

All in all, the two independent estimates agree. Therefore, we consider that the plasma in the chamber drifts with velocity in the range 1–15 km/s, where 15 km/s is to be considered its upper theoretical limit (given V_A).

Appendix B: Setting Parameters for Our Numerical Simulations

In Table B1 we list the setting parameters defining our numerical simulations.

FS, MS, and CH refer to Frequency Sweep, Multi-Spectral and CHirp instrumental modes, respectively. As discussed in Section 4.3, to obtain one measurement for the frequency sweep and multi-spectral modes multiple runs (i.e., 39 and 6 runs, respectively) were needed. For the chirp mode only one run was performed. Since to the different runs of the same instrumental measurement corresponds the same perturbed plasma, we simplified Table B1 by only giving for each measurement the details of the simulations related to the first and last emitted frequencies. The details regarding the remaining simulations can be extrapolated from Table B1 by using the frequency resolution of the measurements (last column).

Table B1
List of Parameters Used to Set Our Numerical Simulations: Total Length of the Simulation Box (X_{max}), Absolute Value of Maximum and Minimum Frequency of the Velocity Range for the Electron Distribution Function ($V_{max,e}$), Amount of Spatial Mesh Points (n_x), Amount of Velocity Mesh Points for Electrons (n_{ve}), Advancement Time Resolution of the Simulation (dt), Emission Frequency (ω), Oscillating Charges at the Antenna (σ), Ion-To-Electron Mass Ratio (m_i/m_e), Ion-To-Electron Temperature Ratio (T_i/T_e), Frequency Sweep Resolution (f_{n+1}/f_n)

Name	$X_{\max}[\lambda_D]$	$v_{\max,e}[v_{the}]$	n_x	n_{v_e}	Dt $[\omega_p^{-1}]$	$\omega[\omega_p]$	$\sigma[\bar{\sigma}]$	$\frac{f_{n+1}}{f_n}$
FS_01	4,000	10	8,192	101	1e−3	0.5	1e−5	1.05
FS_39	4,000	10	8,192	101	1e−3	0.5	1e−5	1.05
MS_01	4,000	10	8,192	101	1e−3	0.5	1e−5	1.05
MS_06	4,000	10	8,192	101	1e−3	0.5	1e−5	1.05
CH_01	4,000	10	8,192	101	1e−3	0.5–5	1e−5	1.05

Data Availability Statement

Datasets for this research are available at Bucciantini (2022), together with a detailed explanation on how to use them.

The model used for the production of such dataset is described in Section 3.1. It is based on the model implemented by Mangeney et al. (2002). The 1D-1V Vlasov-Poisson version of the model, which corresponds to the one we use in our investigation, is described in Henri et al. (2010).

Acknowledgments

The work performed at LPC2E is supported by CNES APR. We benefited from the computing resources provided by CaSciModOT. This work was granted access to the HPC/AI resources of TGCC under the allocation 2021-A0100412428 made by GENCI. L.B. was supported by funds from Région Centre Val de Loire (France).

We thank E. Odelstad for the support he provided for the identification of the plasma drift velocity in the chamber.

References

Bahnsen, A., Jespersen, M., Ungstrup, E., Pottelette, R., Malingre, M., Decreau, P., et al. (1988). First VIKING results: High frequency waves. *Physica Scripta*, *37*(3), 469–474. https://doi.org/10.1088/0031-8949/37/3/032

Béghin, C. (1995). Series expansion of electrostatic potential radiated by a point source in isotropic Maxwellian plasma. *Radio Science*, *30*(2), 307–322. https://doi.org/10.1029/94RS03167

Béghin, C., & Debrie, R. (1972). Characteristics of the electric field far from and close to a radiating antenna around the lower hybrid resonance in the ionospheric plasma. *Journal of Plasma Physics*, *8*(3), 287–310. https://doi.org/10.1017/S0022377800007157

Béghin, C., Karczewski, J. F., Poirier, B., Debrie, R., & Masevich, N. (1982). The ARCAD-3 ISOPROBE experiment for high time resolution thermal plasma measurements. *Annales de Geophysique*, *38*(5), 615–629.

Bucciantini, L. (2022). nov) New high time resolution mutual impedance measurements. *Zenodo*. https://doi.org/10.5281/zenodo.7278491

Bucciantini, L., Henri, P., Wattieaux, G., Califano, F., Vallières, X., & Randriamboarison, O. (2022). In situ space plasma diagnostics with finite amplitude active electric experiments: Non-linear plasma effects and instrumental performance of mutual impedance experiments. *JGR: Space Physics*, *127*(12). https://doi.org/10.1029/2022ja030813

Chasseriaux, J., Debrie, R., & Renard, C. (1972). Electron density and temperature measurements in the lower ionosphere as deduced from the warm plasma theory of the h.f. quadrupole probe. *Journal of Plasma Physics*, *8*(2), 231–253. https://doi.org/10.1017/S0022377800007108

Chasseriaux, J. M. (1972). Potential set up by a point charge oscillating in magnitude in an inhomogeneous plasma. *Plasma Physics*, *14*(8), 763–781. https://doi.org/10.1088/0032-1028/14/8/002

Chasseriaux, J. M. (1974). Excitation of the plasma and upper hybrid resonances in a warm magnetoplasma by an alternating electric dipole. *Journal of Plasma Physics*, *11*(2), 225–252. https://doi.org/10.1017/S0022377800024624

Décréau, P. M. E., Beghin, C., & Parrot, M. (1978). Electron density and temperature, as measured by the mutual impedance experiment on board GEOS-1 (Article published in the special issues: Advances in Magnetospheric Physics with GEOS- 1 and ISEE - 1 and 2. *Space Science Reviews*, *22*(5), 581–595. https://doi.org/10.1007/BF00223942

Gargioni, E., & Grosswendt, B. (2008). Electron scattering from argon: Data evaluation and consistency. *Reviews of Modern Physics*, *80*(2), 451–480. https://doi.org/10.1103/RevModPhys.80.451

Geiswiller, J., Béghin, C., Kolesnikova, E., Lagoutte, D., Michau, J. L., & Trotignon, J. G. (2001). Rosetta spacecraft influence on the mutual impedance probe frequency response in the long Debye length mode. *Planetary and Space Science*, *49*(6), 633–644. https://doi.org/10.1016/S0032-0633(00)00173-2

Gilet, N., Henri, P., Wattieaux, G., Cilibrasi, M., & Béghin, C. (2017). Electrostatic potential radiated by a pulsating charge in a two-electron temperature plasma. *Radio Science*, *52*(11), 1432–1448. https://doi.org/10.1002/2017RS006294

Gilet, N., Henri, P., Wattieaux, G., Myllys, M., Randriamboarison, O., Béghin, C., & Rauch, J.-L. (2019). Mutual impedance probe in collisionless unmagnetized plasmas with suprathermal electrons—Application to BepiColombo. *Frontiers in Astronomy and Space Sciences*, *6*. https://doi.org/10.3389/fspas.2019.00016

Grard, R. (1969). Coupling between two electric aerials in a warm plasma. *Alta Frequency*, *38*, 97–101.

Grard, R. (1997). Influence of suprathermal electrons upon the transfer impedance of a quadrupolar probe in a plasma. *Radio Science*, *32*(3), 1091–1100. https://doi.org/10.1029/97RS00254

Henri, P., Califano, F., Briand, C., & Mangeney, A. (2010). Vlasov-Poisson simulations of electrostatic parametric instability for localized Langmuir wave packets in the solar wind. *Journal of Geophysical Research*, *115*(A6), A06106. https://doi.org/10.1029/2009JA014969

Kasaba, Y., Kojima, H., Moncuquet, M., Wahlund, J., Yagitani, S., Sahraoui, F., et al. (2020). Plasma wave investigation (PWI) aboard Bepi-Colombo mio on the trip to the first measurement of electric fields, electromagnetic waves, and radio waves around mercury. *Space Science Reviews*, *216*(65), 65. https://doi.org/10.1007/s11214-020-00692-9

Kaufman, H. R., Cuomo, J. J., & Harper, J. M. E. (1982). Technology and applications of broad-beam ion sources used in sputtering. part i. ion source technology. *Journal of Vacuum Science and Technology*, *21*(3), 725–736. https://doi.org/10.1116/1.571819

Mangeney, A., Califano, F., Cavazzoni, C., & Travnicek, P. (2002). A numerical scheme for the integration of the Vlasov-Maxwell system of equations. *Journal of Computational Physics*, *179*(2), 495–538. https://doi.org/10.1006/jcph.2002.7071

Odelstad, E., Eriksson, A. I., Johansson, F. L., Vigren, E., Henri, P., Gilet, N., et al. (2018). Ion velocity and electron temperature inside and around the diamagnetic cavity of comet 67P. *Journal of Geophysical Research: Space Physics*, *123*(7), 5870–5893. https://doi.org/10.1029/2018JA025542

Pottelette, R., Rooy, B., & Fiala, V. (1975). Theory of the mutual impedance of two small dipoles in a warm isotropic plasma. *Journal of Plasma Physics*, *14*(2), 209–243. https://doi.org/10.1017/S0022377800009533

Pottelette, R., & Storey, L. R. O. (1981). Active and passive methods for the study of non-equilibrium plasmas using electrostatic waves. *Journal of Plasma Physics*, *25*(2), 323–350. https://doi.org/10.1017/S0022377800023151

Ranvier, S., Anciaux, M., De Keyser, J., Pieroux, D., Baker, N., & Lebreton, J.-P. (2019). Slp: The sweeping Langmuir probe instrument to monitor the upper ionosphere on board the PICASSO nano-satellite.

Retinò, A., Khotyaintsev, Y., Le Contel, O., Marcucci, M. F., Plaschke, F., Vaivads, A., et al. (2021). Particle energization in space plasmas: Towards a multi-point, multi-scale plasma observatory. *Experimental Astronomy*. https://doi.org/10.1007/s10686-021-09797-7

Rooy, B., Feix, M. R., & Storey, L. R. O. (1972). Theory of a quadripolar probe for a hot isotropic plasma. *Plasma Physics*, *14*(3), 275–300. https://doi.org/10.1088/0032-1028/14/3/005

Snodgrass, C., & Jones, G. H. (2019). The European Space Agency's Comet interceptor lies in wait. *Nature Communications*, *10*(5418), 5418. https://doi.org/10.1038/s41467-019-13470-1

Storey, L., Aubry, L., & Meyer, P. (1969). Mutual impedance techniques for space plasma measurements. *Measurement techniques in space plasmas - Fields Geophysical Monograph Series*, *103*, 155–160. https://doi.org/10.1029/GM103p0155

Trotignon, J., Béghin, C., Lagoutte, D., Michau, J., Matsumoto, H., Kojima, H., et al. (2006). Active measurement of the thermal electron density and temperature on the mercury magnetospheric orbiter of the BepiColombo mission. *Advances in Space Research*, *38*(4), 686–692. https://doi.org/10.1016/j.asr.2006.03.031

Trotignon, J., Michau, J. L., Lagoutte, D., Chabassière, M., Chalumeau, G., Colin, F., et al. (2007). RPC-MIP: The mutual impedance probe of the rosetta plasma consortium. *Space Science Reviews*, *128*(1–4), 713–728. https://doi.org/10.1007/s11214-006-9005-1

Wattieaux, G., Gilet, N., Henri, P., Vallières, X., & Bucciantini, L. (2019). Rpc-mip observations at comet 67P/Churyumov-Gerasimenko explained by a model including a sheath and two populations of electrons. *Astronomy & Astrophysics*, *630*, A41. https://doi.org/10.1051/0004-6361/201834872

Wattieaux, G., Henri, P., Gilet, N., Vallières, X., & Deca, J. (2020). Plasma characterization at comet 67P between 2 and 4 au from the Sun with the RPC-MIP instrument. *Astronomy & Astrophysics*, *638*, A124. https://doi.org/10.1051/0004-6361/202037571